Nigerian Journal of Physics (NJP)
ISSN online: 3027-0936
ISSN print: 1595-0611
DOI: https://doi.org/10.62292/njp.v33i2.2024.215
Volume 33(2), June 2024

The Study of Lead-Free $CH_3NH_3GeX_3$ (X=F, Cl, Br, I and At) for Optoelectronic Applications Using First-Principle

***Abdulsalam H. and Abdullahi T.**

Department of Physics, Yobe State University, P.M.B.1144 Damaturu, Yobe Nigeria

*Corresponding author's email: ahassanabdulsalam@gmail.com

ABSTRACT

Organometallic perovskites, with their exceptional electric, magnetic, piezoelectric, and optical properties, are prominent in materials science research. The environmental and health concerns associated with lead-based perovskites have spurred the search for lead-free alternatives, such as methylammonium germanium halides. This study investigates the optical and electronic properties of organometallic perovskite materials, focusing on methylammonium germanium halides ($CH_3NH_3GeX_3$, where X = F, Cl, Br, I, At). Using computational methods, the analysed properties including band gap energies, dielectric constants, extinction coefficients, optical conductivity, absorption coefficients, reflectivity, refractive indices, and lattice constants. The results show a decreasing trend in band gap energies from 3.987 eV ($CH_3NH_3GeF_3$) to 0.821 eV ($CH_3NH_3GeAt_3$), indicating weaker bonding interactions with larger halide ions. Lattice constants increase from 4.981 Å ($CH_3NH_3GeF_3$) to 6.068 Å ($CH_3NH_3GeAt_3$), reflecting the larger ionic radii of the heavier halides. $CH_3NH_3GeI_3$ displayed the highest dielectric constant, demonstrating a strong response to external electric fields. Extinction coefficients were significant within the 0 to 10 eV frequency range, with $CH_3NH_3GeI_3$ showing the highest values. Optical conductivity peaked in $CH_3NH_3GeI_3$, suggesting its potential for photovoltaic and light-emitting applications. The absorption coefficients indicated strong visible range absorption for CH3NH3GeI3. Reflectivity analysis revealed that $CH_3NH_3GeF_3$ and $CH_3NH_3GeCl_3$ had higher static reflectivity, suitable for applications requiring minimal reflection, whereas $CH_3NH_3GeI_3$ exhibited minimal reflection, beneficial for high-efficiency photovoltaic cells. The refractive index analysis showed that $CH_3NH_3GeI_3$ had the highest static refractive index, indicating significant optical density and light-slowing capabilities. These findings highlight the relationship between halide substitution and the optical properties of organometallic perovskite materials, providing insights for tailored technological applications.

Keywords:
Organometallic perovskite,
Halide substitution,
Density functional theory (DFT),
Band structure analysis,
Optical properties.

INTRODUCTION

Organometallic perovskite materials exhibit the typical structure of AMX3 perovskites, with X representing the halide, M representing the metal, and the remaining cation position, A, being occupied by an organic molecule; Methylammonium (CH_3NH_3). These perovskites are highly intriguing in the realm of materials science due to their noteworthy electric, magnetic, piezoelectric, optical, and other inherent properties (Yuan et al., 2015). In recent years, metal halide perovskite solar cells have significantly transformed the future potential of next-generation photovoltaic cells. With the rapid advancement of this technology, investigating its environmental impact is gaining importance. One notable disadvantage of metal halide perovskites in their present form is their heavy metal content (Babayigit et al., 2016). Unfortunately, the most efficient perovskite solar cells all incorporate lead (Pb), a concerning drawback that raises significant environmental issues. This poses a major obstacle to their widespread application (Babayigit et al., 2016). Regulations and common sense indicate that perovskite solar cells must become lead-free to provide a truly sustainable technology (Abate, 2017). Given these facts, the development of a lead-free halide perovskite that can rival lead-based halide perovskite is of exceptional interest.

The rising interest in lead-free organometallic perovskites stems from their potential as environmentally friendly substitutes for $CH_3NH_3PbI_3$ in the development of advanced solar cells. A noteworthy contender in this domain is $CH_3NH_3GeI_3$, which has recently garnered attention as a promising candidate for non-toxic photovoltaic applications. The significance of $CH_3NH_3GeI_3$ lies in its use of germanium, an element belonging to the same group as lead and tin. This chemical affinity not only contributes to the material's favourable properties but also positions it as a viable alternative in the ongoing pursuit of eco-friendly and sustainable solar cell technologies (Lu et al., 2016).

This study aims to investigate the substitution of iodide (I) in $CH_3NH_3GeI_3$ with alternative halides, namely fluoride (F), chloride (Cl), bromide (Br), and astatine (At). Employing a first-principle approach, we will conduct an in-depth examination of the impact of halide substitution on the geometric, electronic, and optical properties of the resulting compounds. This investigation will be carried out through the application of density functional theory (DFT), utilizing the FHI-aims package for accurate and comprehensive simulations(Blum et al., 2009). By systematically exploring the variations introduced by different halides, we seek to gain insights into the structural, electronic, and optical behavaior of the modified perovskite, offering valuable information for the advancement of materials in the realm of semiconductor and optoelectronic applications

MATERIALS AND METHODS

Computational Details

In the computational phase of this study, we employed state-of-the-art methods to investigate the impact of halide substitution on $CH_3NH_3GeI_3$. The following outlines the computational details of the study:

Halide Substitution

The systematic replacement of iodide (I) in $CH_3NH_3GeI_3$ with fluoride (F), chloride (Cl), bromide (Br), and astatine (At) resulted in four different materials; $CH_3NH_3GeF_3$, $CH_3NH_3GeCl_3$, $CH_3NH_3GeBr_3$ and $CH_3NH_3GeAt_3$

Electronic Structure Calculations

The study utilized density functional theory (DFT) implemented in the FHI-aims package for accurate electronic structure calculations. Parameters such as occupation type, charge mix, initial moment, and nmax Pulay were optimized to minimize energy and achieve convergence within a reasonable computational time for each material. Various guesses were made to facilitate convergence, ensuring efficiency without sacrificing accuracy in the simulations.

Geometry Optimization, Equilibrium Lattice Constant and k-grid Convergence Test

After the replacement of iodide with different halides, each resulting material would undergo geometry optimization. Therefore, each of the four materials would individually undergo geometry optimization in separate simulations to determine their respective optimized atomic structures and minimum energy configurations. To determine the geometric properties of the studied compounds, geometry optimization calculations were performed. The atomic positions were adjusted iteratively until the forces on each atom were minimized, indicating convergence to the minimum energy structure. Single-point energy calculations were conducted for each structure while systematically varying the lattice constants. Convergence tests were executed for k-grids of 3x3x3, 6x6x6, 9x9x9, and 12x12x12. Through these calculations, the equilibrium lattice constant and the optimal k-grid size corresponding to the minimum ground state energy were determined.

Band Structure Analysis

Utilizing the optimized parameters obtained from geometry optimization, band structure analysis was carried out. High symmetry points in reciprocal space were defined and tagged in the control.in file. The band structure was then analysed to elucidate the electronic properties of each material.

Complex Dielectric Function and Optical Properties Calculation

The complex dielectric function was derived using the compute_dielectric calculation, which enabled the computation of both the imaginary and real parts of the inter-band and intra-band contributions. These calculations were performed for the [111] crystallographic direction. Based on the obtained complex dielectric function, the optical properties, including the refractive index ($n(\omega)$), extinction coefficient ($k(\omega)$), absorption coefficient ($\alpha(\omega)$), reflectivity ($R(\omega)$), and optical conductivity ($\sigma(\omega)$) were subsequently determined(Saha et al., 2000). This comprehensive analysis enabled a thorough understanding of the material's optical behavaior across different directions.

i. The absorption coefficient, $\alpha(\omega)$, indicates the extent to which light of a specific wavelength is absorbed by a material. Materials with low absorption coefficients appear transparent to that wavelength, especially when they are thin. The absorption coefficient is influenced by both the material's properties and the wavelength of the incident light (Wang, 2008).

$$\alpha(\omega) = \frac{\sqrt{2}\,\omega}{c}\sqrt{\left(\sqrt{\left(\varepsilon_1(\omega)\right)^2 + \left(\varepsilon_2(\omega)\right)^2}\right) - \varepsilon_1(\omega)} \quad (1)$$

ii. The optical conductivity, σ(ω), describes the relationship between the current density and the electric field across a material for various frequencies. It encompasses a broader frequency range compared to electrical conductivity (Gervais, 2002).

$$\sigma(\omega) = \frac{\omega}{4\pi}\varepsilon_2(\omega) \quad (2)$$

iii. The extinction coefficient, k(ω gauges the decrease in transmitted light due to scattering and absorption in a medium, indicating the attenuation of an electromagnetic wave as it travels through the medium (Valizade et al., 2019).

$$k(\omega) = \sqrt{\frac{\sqrt{\left(\varepsilon_1(\omega)\right)^2 + \left(\varepsilon_2(\omega)\right)^2} - \varepsilon_1(\omega)}{2}} \quad (3)$$

iv. Reflectivity, R(ω) quantifies the fraction of incident light reflected from a material's surface relative to the incident light intensity, reflecting the material's ability to reflect light both at the surface and within its volume (Ujihara, 1972).

$$R(\omega) = \frac{(n(\omega)-1)^2 + k(\omega)^2}{(n(\omega)+1)^2 + k(\omega)^2} \quad (4)$$

v. The refractive index, n(ω), quantifies the degree of light bending as it transitions between different media, representing the ratio of light velocity in a vacuum to its velocity in a substance (Afromowitz, 1974), indicating the medium's optical density.

$$n(\omega) = \sqrt{\frac{\sqrt{\left(\varepsilon_1(\omega)\right)^2 + \left(\varepsilon_2(\omega)\right)^2} + \varepsilon_1(\omega)}{2}} \quad (5)$$

RESULTS AND DISCUSSION

Bandgap and Lattice Constant

Table 1 provides detailed information on the band gap energies and lattice constants for a series of organometal halide perovskites with the chemical formula $CH_3NH_3GeX_3$, where X represents different halogens (F, Cl, Br, I, At). These materials are of interest for their potential applications in optoelectronic devices.

Table 1: Bandgap and lattice constant

Material	Band Gap (eV)		Lattice constant (Å)	
	This work	Reported Values	This work	Reported Values
$CH_3NH_3GeF_3$	3.98763259		5.903	
$CH_3NH_3GeCl_3$	3.80044950		5.920	
$CH_3NH_3GeBr_3$	1.91664789		5.845	
$CH_3NH_3GeI_3$	1.60609577	1.54(Yuqiu et al., 2017)2.0(Hoefler et al., 2017)1.60 (Umadevi & Watson, 2019)	5.740	6.183 (Stoumpos & Kanatzidis, 2015) 5.907(Umadevi & Watson, 2019)
$CH_3NH_3GeAt_3$	0.82064682		5.900	

From Table 1, $CH_3NH_3GeF_3$ exhibits the highest band gap at approximately 3.99 eV, suggesting it is less suitable for applications requiring narrow band gaps but could be useful for UV light applications. $CH_3NH_3GeCl_3$ shows a slightly lower band gap of about 3.80 eV, indicating a minor reduction in energy difference compared to the fluoride variant. $CH_3NH_3GeBr_3$ has a significantly lower band gap of 1.92 eV, making it more suitable for visible light absorption, which is beneficial for applications like solar cells and LEDs. CH_3NH_3GeI displays a band gap of approximately 1.61 eV, aligning closely with previously reported values ranging from 1.54 eV to 2.0 eV. This narrow band gap is ideal for absorbing a wide spectrum of visible light, enhancing its application in photovoltaic devices. $CH_3NH_3GeAt_3$ possesses the lowest band gap of approximately 0.82 eV, indicating potential for infrared applications but also suggesting challenges with stability and synthesis.

The lattice constant values provide insight into the structural dimensions of the crystal lattice, which influences the material's electronic properties and stability. $CH_3NH_3GeF_3$ has a lattice constant of 5.903 Å, indicating a relatively compact structure. $CH_3NH_3GeCl_3$ shows a lattice constant of 5.920 Å, slightly larger than the fluoride variant, reflecting the larger size of chlorine atoms compared to fluorine. $CH_3NH_3GeBr_3$ exhibits a lattice constant of 5.845 Å, which is somewhat surprising as bromine is larger than chlorine, yet it shows a slightly smaller lattice constant. This could be due to structural relaxation effects or measurement uncertainties. $CH_3NH_3GeI_3$ displays a variable lattice constant with reported values ranging from 5.740 Å to 6.183 Å. The variability in reported values might stem from different synthesis methods or measurement conditions. The value from this work is 5.907 Å, which falls within the reported range and suggests a mid-range lattice constant size among the halides. $CH_3NH_3GeAt_3$ has a lattice constant of 5.900 Å, indicating a structure size similar to $CH_3NH_3GeF_3$ and $CH_3NH_3GeCl_3$, despite the much larger atomic size of astatine. This could

suggest significant structural adjustments or specific bonding characteristics unique to astatine.

The data shows a clear trend where the band gap decreases as the halogen changes from F to At (Hutter et al., 2015), which is consistent with the increasing atomic size and decreasing electronegativity of the halogens. This trend is important for tuning the optical properties of these materials for specific applications. The lattice constants do not show a simple linear trend with halogen size, indicating complex interactions within the crystal structure. This nuanced understanding is crucial for tailoring material properties through chemical substitutions in the perovskite structure.

Examining the dataset in Table 1, a notable correlation emerges between the lattice constant and band gap of the organometal halide perovskites studied. Progressing from $CH_3NH_3GeF_3$ to $CH_3NH_3GeAt_3$ reveals a consistent pattern: the band gap decreases alongside a slight decrease in lattice constant. For instance, $CH_3NH_3GeF_3$ exhibits the highest band gap (3.99 eV) with a lattice constant of 5.903 Å, while $CH_3NH_3GeAt_3$ displays the lowest band gap (0.82 eV) with a lattice constant of 5.900 Å. This inverse relationship aligns with semiconductor physics principles, where larger lattice constants typically result in narrower band gaps due to weakened electron confinement (Makin et al., 2020). However, $CH_3NH_3GeI_3$ slightly deviates from this trend. Despite its relatively larger lattice constant (5.907 Å), its band gap (1.61 eV) is not the lowest among the compounds, indicating additional factors at play.

Dielectric Constant

The dielectric constant (relative permittivity) is value of the real part of the linear dielectric constant at frequency equals to zero (i.e. $Re[\epsilon_r(\omega = 0)]$).

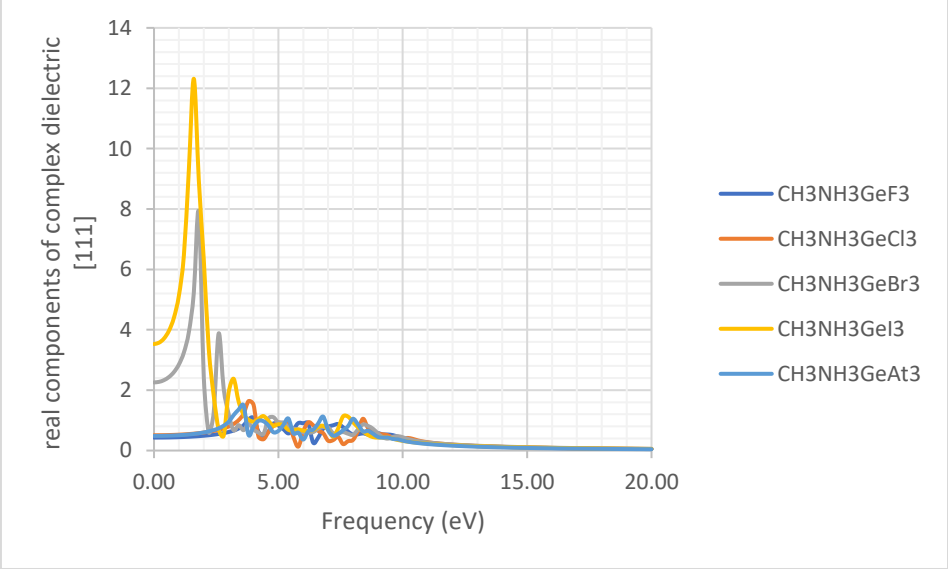

Figure 1: Graph of real components of complex dielectric function against Frequency

The data in Table 2 were extracted from the graph of real components of linear dielectric function against frequency function in Figure 1, reveals varying magnitudes of dielectric constants among the studied materials

Table 2: Dielectric Constant (ϵ)

Material	Dielectric constant $Re[\epsilon_r(\omega = 0)]$[111] Direction
$CH_3NH_3GeF_3$	0.429191366
$CH_3NH_3GeCl_3$	0.506642891
CH_3NH_3 $GeBr_3$	2.256186281
$CH_3NH_3GeI_3$	3.528300503
$CH_3NH_3GeAt_3$	0.484651426

$CH_3NH_3GeI_3$ demonstrates considerably higher dielectric constants compared to $CH_3NH_3GeF_3$ and $CH_3NH_3GeCl_3$ across all crystallographic directions. This suggests a stronger response to external electric fields in $CH_3NH_3GeI_3$, likely attributed to its specific crystal structure and electronic configuration. Furthermore, a clear directional dependence is observed in the dielectric constants. For instance, $CH_3NH_3GeBr_3$

exhibits a substantial increase in dielectric constant along the [001] direction compared to the other directions, indicating anisotropic behavaior in its response to electric fields. Similarly, $CH_3NH_3GeCl_3$ displays the highest dielectric constant in the [001] direction, indicating preferential polarization along this axis. Interestingly, $CH_3NH_3GeF_3$ shows relatively lower dielectric constants across all crystallographic directions compared to the other materials. This characteristic may stem from its unique molecular arrangement and interactions within the crystal lattice, resulting in diminished polarization effects.

Extinction Coefficient k(ω)

The extinction coefficients (k(ω)) for all materials demonstrate significant activity primarily within the 0 to 10 eV frequency range, with multiple peaks observed between 1 and 8 eV.

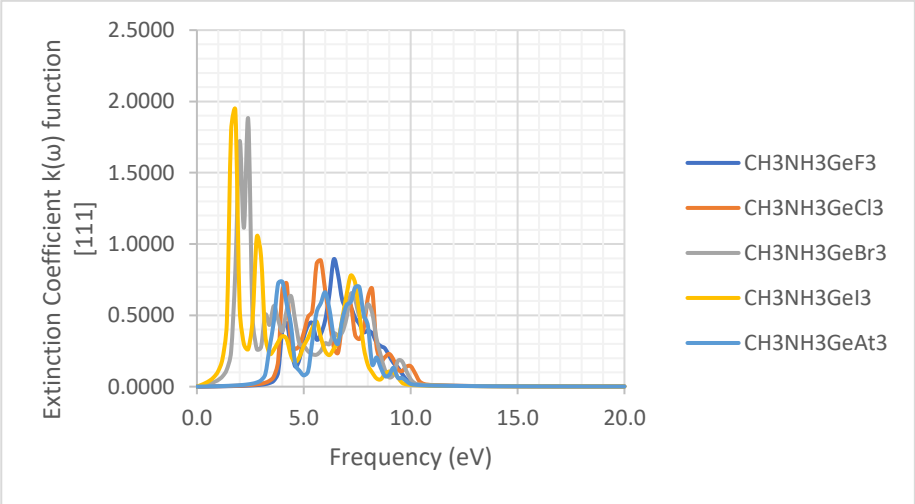

Figure 2: Graph of Extinction Coefficient k(ω) function against Frequency

The extinction coefficient peaks in Table 3 were obtained from Figure 2; graphs of extinction coefficient k(ω) function against frequency

Table 3: Extinction Coefficients Peak Positions and Intensities

Material	Peak Positions (eV)	Peak Intensities
$CH_3NH_3GeF_3$	2 - 5	Moderate
$CH_3NH_3GeCl_3$	3 - 6	Slightly higher than $CH_3NH_3GeF_3$
$CH_3NH_3GeBr_3$	2 - 6	Higher than $CH_3NH_3GeF_3$ and $CH_3NH_3GeCl_3$
$CH_3NH_3GeI_3$	2 - 4	Highest peaks, prominent peak > 2
$CH_3NH_3GeAt_3$	2 - 4	Slightly different intensities and positions

At lower frequencies (below 2 eV), the extinction coefficient exhibits rapid increases, indicating strong absorption in the visible to near-infrared region. As the frequency increases beyond 8 eV, the extinction coefficients for all materials tend to decrease and stabilize, indicating reduced absorption in the ultraviolet range. $CH_3NH_3GeI_3$ shows the highest extinction coefficients and the most pronounced peaks, suggesting it has the strongest absorption in the visible range. $CH_3NH_3GeBr_3$ also demonstrates significant peaks, indicating a high absorption capacity. In contrast, $CH_3NH_3GeF_3$ and $CH_3NH_3GeCl_3$ display more moderate and lower extinction coefficients, suggesting they are less absorbing compared to their bromine and iodine counterparts. The trends observed in the extinction coefficient align with those in dielectric constants and refractive indices, where higher values correlate with stronger absorption characteristics.

High absorption materials like $CH_3NH_3GeI_3$ and $CH_3NH_3GeBr_3$ are suitable for applications requiring strong absorption in the visible range, such as solar cells, photodetectors, and other optoelectronic devices(Wu et al., 2023). Conversely, materials with lower and more stable absorption characteristics like $CH_3NH_3GeF_3$ and $CH_3NH3GeCl_3$ might be better suited for applications demanding consistent performance with minimal absorption, such as transparent conducting films or protective coatings (Chen et al., 2017).

Optical conductivity σ(ω)

The Table 4 presents the peak positions and intensities of optical conductivity. The peak positions indicate the

energy levels at which significant optical conductivity occurs, while the intensity reflects the magnitude of this conductivity (Palik, 1998) (Dresselhaus et al., 2007). The peak optical conductivities in Table 4 were obtained from Figure 3.

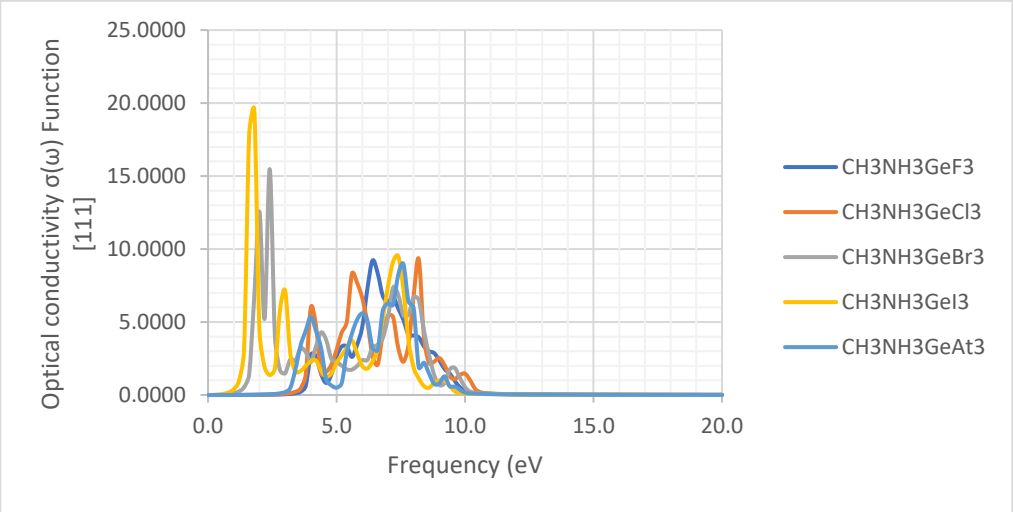

Figure 3: Graph of Optical Conductivity σ(ω) function against Frequency

Table 4: Peak Positions and Intensities of Optical Conductivity

Material	Peak Position (eV)	Intensity
$CH_3NH_3GeF_3$	3-5	Low
$CH_3NH_3GeCl_3$	3-8	Moderate to High
$CH_3NH_3GeBr_3$	3-9	Moderate to High
$CH_3NH_3GeI_3$	4-5, up to 10	Highest
$CH_3NH_3GeAt_3$	3-10	High

For $CH_3NH_3GeF_3$, the peak positions range from 3-5 eV with low intensity, indicating lower optical conductivity compared to other halogens, with significant activity primarily between 3-5 eV. This makes $CH_3NH_3GeF_3$ suitable for applications where lower optical conductivity is desired, such as in anti-reflective coatings or devices where minimal light reflection is beneficial. $CH_3NH_3GeCl_3$ shows peaks between 3-8 eV with moderate to high intensity, demonstrating increased optical activity as the halogen size increases. This compound is suitable for optical sensors and detectors that require higher sensitivity and broader detection ranges, reflecting its strong interaction with light. $CH_3NH_3GeBr_3$ has peaks spanning 3-9 eV with moderate to high intensity, indicating a broader range of optical activity. This makes it effective for use in broadband optical devices that need to operate across a wide spectrum of light frequencies. $CH_3NH_3GeI_3$ exhibits the highest intensity peaks, with positions between 4-5 eV and extending up to 10 eV, indicating a strong optical response at specific frequencies. Its high intensity and broad range make it highly suitable for high-efficiency photovoltaic cells and light-emitting devices, enhancing their ability to convert light into electricity or emit light with high intensity. $CH_3NH_3GeAt_3$, with peaks from 3-10 eV and high intensity, follows the trend of larger halogens having higher optical activity. This compound can be utilized in advanced optical and electronic components where high optical activity and a broader frequency range are crucial, such as in advanced photodetectors, modulators, and other high-performance optoelectronic devices.

All compounds display significant optical conductivity below 10 eV, with intensity and peak positions varying among them. Beyond 10 eV, optical conductivity drops significantly for all compounds. The trends indicate that smaller halogens such as fluorine and chlorine result in lower intensity and a narrower range of optical conductivity, whereas larger halogens like bromine, iodine, and astatine enhance optical conductivity, both in intensity and frequency range. The peak positions shift to lower frequencies (redshift) as the atomic number of the halogen increases. $CH_3NH_3GeI_3$ exhibits the highest peak intensities, indicating the strongest optical conductivity, while $CH_3NH_3GeCl_3$ and $CH_3NH_3GeBr_3$ have similar profiles with varying intensities and positions. $CH_3NH_3GeF_3$ shows the least intense optical conductivity peaks (Stoumpos & Kanatzidis, 2016).

Absorption coefficient α(ω)

The absorption coefficients for all materials show significant activity primarily in the frequency range of 0 to 12 eV, with multiple peaks observed between 3 and 10 eV (Figure 4).

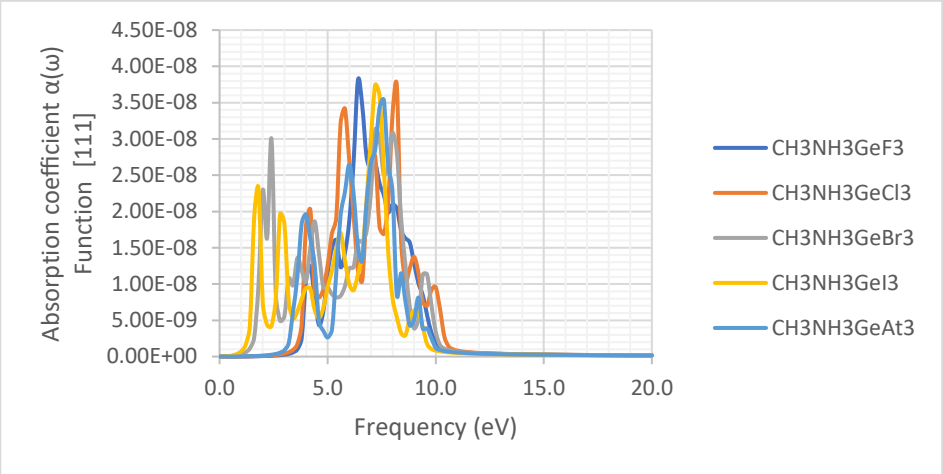

Figure 4: Graph of Absorption coefficient α(ω)function against Frequency

The absorption coefficient Peak positions and intensities in Table 5 were obtained from Figure 4; a graph of absorption coefficient α(ω)function against frequency.

Table 5: Peak Absorption Coefficients

Material	Peak Positions (eV)	Peak Intensities
$CH_3NH_3GeF_3$	4.5 - 7.5	Moderate
$CH_3NH_3GeCl_3$	5 - 8	Slightly higher than CH3NH3GeF3
$CH_3NH_3GeBr_3$	4.5 - 6.5, 7 - 9	Higher than CH3NH3GeF3 and CH3NH3GeCl3
$CH_3NH_3GeI_3$	5 - 8, 9	High
$CH_3NH_3GeAt_3$	4 - 6, 7 - 9	Similar to CH3NH3GeI3 but with slightly different intensities

This Table 5 captures the key peak positions and relative intensities of the absorption coefficients for the different halides. The absorption coefficients for $CH_3NH_3GeF_3$ exhibit several moderate intensity peaks between 4.5 and 7.5 eV. $CH_3NH_3GeCl_3$ displays peaks at similar positions but with slightly higher intensities, particularly between 5 and 8 eV. For $CH_3NH_3GeBr_3$, prominent peaks are observed around 4.5 to 6.5 eV and 7 to 9 eV, with intensities surpassing those of $CH_3NH_3GeF_3$ and $CH_3NH_3GeCl_3$. $CH_3NH_3GeI_3$ features multiple high-intensity peaks, especially between 5 and 8 eV, with another significant peak near 9 eV. $CH_3NH_3GeAt_3$ shows strong absorption peaks around 4 to 6 eV and 7 to 9 eV, similar to $CH_3NH_3GeI_3$ but with slight variations in intensity. $CH_3NH_3GeBr_3$ and $CH_3NH_3GeI_3$, with their high absorption coefficients and strong peaks, could be promising candidates for photovoltaic and optoelectronic applications where efficient light absorption is crucial (Chouhan et al., 2020). Their high absorption in the 5 to 8 eV range makes them particularly suitable for these purposes. On the other hand, $CH_3NH_3GeF_3$ and $CH_3NH_3GeCl_3$, displaying more moderate and stable absorption characteristics, might be better suited for applications requiring consistent and lower absorption, such as in certain dielectric or insulating layers. These materials can provide stable performance in applications where excessive absorption could be detrimental.

Reflectivity R(ω)

Static Reflectivity is the value of the reflectivity R(ω) function at frequency equals to zero i.e., R(ω=0), it is a critical parameter in understanding how materials interact with light at zero frequency(Mistrik et al., 2017). Static Reflectivity $R(\omega = 0)$ in Table 5 were obtained from the graphs of Reflectivity R(ω) function against frequency in Figure 6.

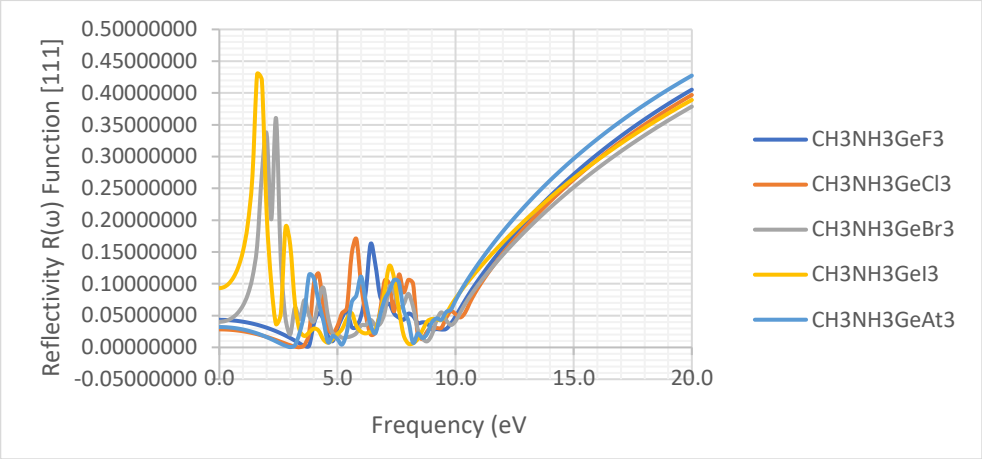

Figure 5: Graph of Reflectivity R(ω) function against Frequency

Table 6: Reflectivity Characteristics

Material	Static Reflectivity	Application
$CH_3NH_3GeF_3$	0.041195	Highly suitable for high reflectivity applications
$CH_3NH_3GeCl_3$	0.029552	Suitable for high reflectivity applications
$CH_3NH_3GeBr_3$	0.003289	Reflects less light, moderate reflectivity applications
$CH_3NH_3GeI_3$	0.002125	Minimal reflection, more transmission or absorption
$CH_3NH_3GeAt_3$	0.002604	Low reflectivity properties

The trend in static reflectivity correlates with the increasing atomic size and polarizability of the halogen atoms (F < Cl < Br < I). Larger and more polarizable halogen atoms contribute to higher reflectivity due to increased interaction with incident light. $CH_3NH_3GeI_3$ and $CH_3NH_3GeBr_3$ have high reflectivity they are better suitable for applications requiring materials with high reflectivity, such as mirrors, reflective coatings, and optical devices where light reflection is desired (Ye et al., 2021). $CH_3NH_3GeF_3$ and $CH_3NH_3GeCl_3$ have low reflectivity they are better suited for applications requiring minimal reflection and more transmission or absorption, such as in anti-reflective coatings and transparent conducting materials (Mehta et al., 2022). At low frequencies (near 0 eV), reflectivity is low for all materials, with significant increases as frequency approaches the visible range. Distinct peaks in reflectivity are observed between 2 and 5 eV for all materials, indicating strong reflection at certain frequencies. $CH_3NH_3GeI_3$ and $CH_3NH_3GeBr_3$ show the highest peak. Reflectivity tends to stabilize or slightly increase beyond 10 eV for all materials, suggesting reduced changes in reflective properties at higher energies.

Refractive Index n(ω)

The static refractive index, defined as the value of the refractive index n(ω) at zero frequency, provides insight into the optical density and light-slowing capability of materials. Optical density refers to the extent to which a material impedes the passage of light. It is directly related to the refractive index of the material. Materials with a high refractive index possess a high optical density, causing light to travel more slowly through them. Conversely, materials with a low refractive index have a low optical density, allowing light to travel faster through them (Burnett, 1927).

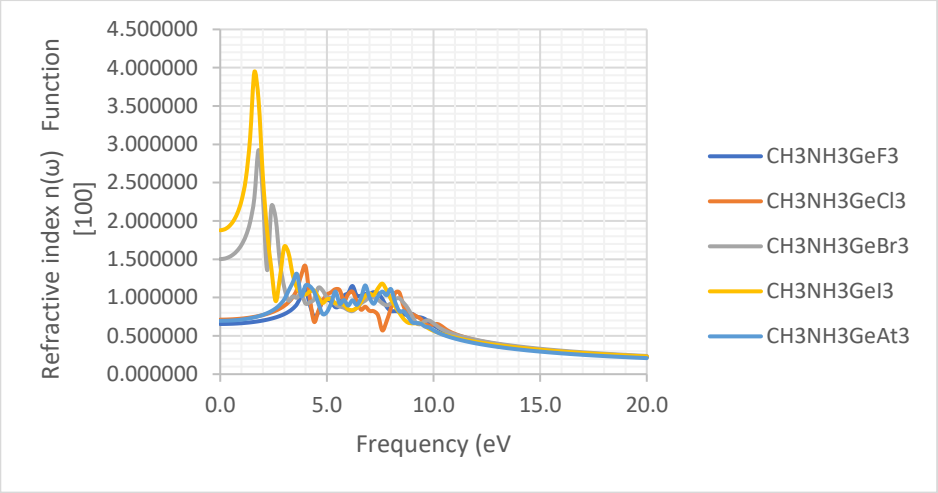

Figure 6: Graph of Refractive Index n (ω) function against Frequency

The static refractive indices for the methylammonium germanium halides ($CH_3NH_3GeX_3$) in Table 7 were obtained from the graph of refractive index n (ω) function against frequency in Figure 5.

Table 7: Static Refractive Index n

Material	Static Refractive Index n(ω=0)
$CH_3NH_3GeF_3$	0.6551
$CH_3NH_3GeCl_3$	0.7118
$CH_3NH_3GeBr_3$	1.5021
$CH_3NH_3GeI_3$	1.8784
$CH_3NH_3GeAt_3$	0.6962

$CH_3NH_3GeF_3$, with a static refractive index of 0.6551, has the lowest optical density. This lower refractive index makes it suitable for applications where minimal light reflection and distortion are necessary, such as in anti-reflective coatings or waveguides. $CH_3NH_3GeCl_3$ has a static refractive index of 0.7118, slightly higher than $CH_3NH_3GeF_3$. This compound is also appropriate for applications requiring lower optical density, offering stability and minimal light distortion in waveguides and substrates. $CH_3NH_3GeBr_3$, with a static refractive index of 1.5021, indicates a higher optical density and enhanced capability to slow down light. This makes it ideal for use in broadband optical devices and photonic components where efficient light manipulation is critical. $CH_3NH_3GeI_3$ exhibits the highest static refractive index at 1.8784, suggesting a significant optical density and strong light-slowing ability. This compound is highly suitable for high-efficiency photovoltaic cells and light-emitting devices, where precise control over light propagation and strong optical responses are required. $CH_3NH_3GeAt_3$ has a static refractive index of 0.6962, which is closer to $CH_3NH_3GeCl_3$. Despite being lower than the indices of bromine and iodine counterparts, it is suitable for advanced optical components requiring stable and lower refractive indices.

The static refractive indices of methylammonium germanium halides reveal a clear trend correlating with the size and polarizability of the halogen atoms: F < Cl < Br < I. Larger and more polarizable halogen atoms contribute to higher refractive indices due to increased electronic polarization under an applied electromagnetic field (Kalyanaraman et al., 2015).

The static refractive indices of methylammonium germanium halides demonstrate a clear trend based on the size and polarizability of the halogen atoms. Compounds with larger halogen atoms, such as iodine and bromine, exhibit higher refractive indices, making them suitable for high-density optical applications. Conversely, compounds with smaller halogen atoms, such as fluorine and chlorine, possess lower refractive indices, providing stability and lower optical density for applications requiring minimal light distortion. These insights are crucial for selecting appropriate materials based on their optical properties for various technological applications (Smith, 2023).

CONCLUSION

The study of methylammonium germanium halides ($CH_3NH_3GeX_3$) reveals significant trends influenced by the halide ions' size and polarizability. As the halide series progresses from fluorine to astatine, band gaps decrease, indicating weaker bonding and reduced energy

gaps with larger ions. Lattice constants increase, reflecting structural adjustments. Dielectric constants show $CH_3NH_3GeI_3$ with the highest value, indicating strong electric field response and directional dependence. Extinction coefficients are significant within the 0 to 10 eV range, with $CH_3NH_3GeI_3$ showing the highest values, making $CH_3NH_3GeI_3$ and $CH_3NH_3GeBr_3$ suitable for solar cells and photodetectors. Lower absorption materials like $CH_3NH_3GeF_3$ and $CH_3NH_3GeCl_3$ are ideal for minimal absorption applications. Optical conductivity increases with larger halogens, with $CH_3NH_3GeI_3$ showing the strongest response, suitable for high-efficiency photovoltaic cells and light-emitting devices. $CH_3NH_3GeF_3$ is suitable for anti-reflective coatings. Absorption coefficients have prominent peaks between 3 and 10 eV, with higher intensities for $CH_3NH_3GeI_3$ and $CH_3NH_3GeBr_3$, indicating potential in photovoltaic and optoelectronic applications. Reflectivity trends show higher static reflectivity for $CH_3NH_3GeF_3$ and $CH_3NH_3GeCl_3$, suitable for mirrors and reflective coatings, while $CH_3NH_3GeI_3$ and $CH_3NH_3GeBr_3$ are better for anti-reflective coatings and transparent conductors. Refractive indices are higher for larger halogens, with $CH_3NH_3GeI_3$ having the highest optical density, making it suitable for high-efficiency photovoltaic cells and light-emitting devices.

In summary, larger halogens enhance optical activity, making these materials suitable for advanced optoelectronic devices, while smaller halogens offer stability and lower absorption, beneficial for consistent performance applications. These findings support targeted material selection based on optical properties for various technologies.

REFERENCES

Abate, A. (2017). Perovskite Solar Cells Go Lead Free. *Joule*. doi:https://doi.org/10.1016/j.joule.2017.09.007

Afromowitz, M. A. (1974). Refractive index of $Ga_{1-x}Al_xAs$. *Solid State Communications, 15*(1), 59-63. doi:https://doi.org/10.1016/0038-1098(74)90014-3

Babayigit, A., Duy Thanh, D., Ethirajan, A., Manca, J., Muller, M., Boyen, H.-G., & Conings, B. (2016). Assessing the toxicity of Pb-and Sn-based perovskite solar cells in model organism Danio rerio. *Scientific reports, 6*(1), 18721.

Blum, V., Gehrke, R., Hanke, F., Havu, P., Havu, V., Ren, X., . . . Scheffler, M. (2009). Ab initio molecular simulations with numeric atom-centered orbitals. *Computer Physics Communications, 180*(11), 2175-2196. doi:https://doi.org/10.1016/j.cpc.2009.06.022

Burnett, D. (1927). *The relation between refractive index and density*. Paper presented at the Mathematical Proceedings of the Cambridge Philosophical Society.

Chen, Y., Sun, H., & Peng, W. (2017). 2D transition metal dichalcogenides and graphene-based ternary composites for photocatalytic hydrogen evolution and pollutants degradation. *Nanomaterials, 7*(3), 62. doi:https://doi.org/10.3390/nano7030062

Chouhan, L., Ghimire, S., Subrahmanyam, C., Miyasaka, T., & Biju, V. (2020). Synthesis, optoelectronic properties and applications of halide perovskites. *Chemical Society Reviews, 49*(10), 2869-2885. doi:https://doi.org/10.1039/c9cs00848a

Dresselhaus, M. S., Dresselhaus, G., & Jorio, A. (2007). *Group theory: application to the physics of condensed matter*: Springer Science & Business Media.

Gervais, F. (2002). Optical conductivity of oxides. *Materials Science and Engineering: R: Reports, 39*(2-3), 29-92. doi:https://doi.org/10.1016/S0927-796X(02)00073-6

Hoefler, S. F., Trimmel, G., & Rath, T. (2017). Progress on lead-free metal halide perovskites for photovoltaic applications: a review. *Monatsh Chem, 148*(5), 795-826. doi:https://doi.org/10.1007/s00706-017-1933-9

Hutter, E. M., Eperon, G. E., Stranks, S. D., & Savenije, T. J. (2015). Charge carriers in planar and meso-structured organic–inorganic perovskites: mobilities, lifetimes, and concentrations of trap states. *The journal of physical chemistry letters, 6*(15), 3082-3090. doi:https://doi.org/10.1021/acs.jpclett.5b01361

Kalyanaraman, S., Shajinshinu, P., & Vijayalakshmi, S. (2015). Refractive index, band gap energy, dielectric constant and polarizability calculations of ferroelectric Ethylenediaminium Tetrachlorozincate crystal. *Journal of Physics and Chemistry of Solids, 86*, 108-113. doi:https://doi.org/10.1016/j.jpcs.2015.07.007

Lu, X., Zhao, Z., Li, K., Han, Z., Wei, S., Guo, C., . . . Wu, C.-m. L. (2016). First-principles insight into the photoelectronic properties of Ge-based perovskites. *RSC advances, 6*(90), 86976-86981. doi:https://doi.org/10.1039/C6RA18534G

Makin, R. A., York, K., Durbin, S. M., & Reeves, R. J. (2020). Revisiting semiconductor band gaps through structural motifs: An Ising model perspective. *Physical Review B, 102*(11), 115202. doi:https://doi.org/10.1103/PhysRevB.102.115202

Mehta, V., Conkel, C., Cochran, A., & Ravindra, N.

(2022). *Materials for Antireflection Coatings in Photovoltaics—An Overview*. Paper presented at the TMS 2022 151st Annual Meeting & Exhibition Supplemental Proceedings.

Mistrik, J., Kasap, S., Ruda, H. E., Koughia, C., & Singh, J. (2017). Optical properties of electronic materials: fundamentals and characterization. *Springer handbook of electronic and photonic materials*, 1-1. doi:https://doi.org/10.1007/978-3-319-48933-9_3

Palik, E. D. (1998). *Handbook of optical constants of solids* (Vol. 3): Academic press.

Saha, S., Sinha, T., & Mookerjee, A. (2000). Electronic structure, chemical bonding, and optical properties of paraelectric BaTiO 3. *Physical Review B*, *62*(13), 8828. doi:https://doi.org/10.1103/PhysRevB.62.8828

Smith, B. (2023). Halogenated Organic Compounds. doi:https://doi.org/10.56530/spectroscopy.vo3774k1

Stoumpos, C. C., & Kanatzidis, M. G. (2015). The renaissance of halide perovskites and their evolution as emerging semiconductors. *Accounts of chemical research*, *48*(10), 2791-2802. doi:https://doi.org/10.1021/acs.accounts.5b00229

Stoumpos, C. C., & Kanatzidis, M. G. (2016). Halide Perovskites: poor Man's high-performance semiconductors. *Advanced Materials*, *28*(28), 5778-5793. doi:https://doi.org/10.1002/adma.201600265

Ujihara, K. (1972). Reflectivity of metals at high temperatures. *Journal of Applied Physics*, *43*(5), 2376-2383. doi:https://doi.org/10.1063/1.1661506

Umadevi, D., & Watson, G. W. (2019). Quasiparticle GW Calculations on lead-free hybrid germanium iodide perovskite $CH_3NH_3GeI_3$ for photovoltaic applications. *ACS omega*, *4*(3), 5661-5669. doi:https://doi.org/10.1021/acsomega.8b03291

Valizade, M., Heyhat, M., & Maerefat, M. (2019). Experimental comparison of optical properties of nanofluid and metal foam for using in direct absorption solar collectors. *Solar Energy Materials and Solar Cells*, *195*, 71-80. doi:https://doi.org/10.1016/j.solmat.2019.01.050

Wang, L. (2008). *Measuring optical absorption coefficient of pure water in UV using the integrating cavity absorption meter*. (Doctor of Philosophy), Texas A&M University. Retrieved from https://oaktrust.library.tamu.edu/bitstream/handle/1969.1/85959/Wang.pdf?sequence=1

Wu, D., Lei, L., Xie, M., Xu, P., & Xu, S. (2023). *High-performance metamaterial light absorption from visible to near-infrared assisted by anti-reflection coating.* Paper presented at the Photonics.

Ye, Z.-T., Ho, W.-T., & Chen, C.-H. (2021). Highly reflective thin-film optimization for full-angle micro-LEDs. *Nanoscale Research Letters*, *16*, 1-12. doi:https://doi.org/10.1186/s11671-021-03611-1

Yuan, Y., Xu, R., Xu, H.-T., Hong, F., Xu, F., & Wang, L.-J. (2015). Nature of the band gap of halide perovskites ABX_3(A= CH_3NH_3,Cs; B = Sn, Pb; X= Cl, Br, I): First-principles calculations. *Chin. Phys. B 24*(11), 5. doi:https://doi.org/10.1088/1674-1056/24/11/116302

Yuqiu, J., Yuanyuan, L., Jia, L., Mang, N., & Zhenqing, Y. (2017). Exploring electronic and optical properties of $CH_3NH_3GeI_3$ perovskite: Insights from the first principles. *Computational and Theoretical Chemistry*, *1114*, 20-24. doi:https://doi.org/10.1016/j.comptc.2017.05.027